A Microwave Passive Topology Based on Simultaneous Injection-Locking and Injection-Pulling for Passive Indoor Sensing Applications

Davi V. Q. Rodrigues
Dept. of Electrical & Computer Engineering
Texas Tech University
Lubbock, TX, 79409, USA
davi.rodrigues@ttu.edu

Changzhi Li
Dept. of Electrical & Computer Engineering
Texas Tech University
Lubbock, TX, 79409, USA
changzhi.li@ttu.edu

***Abstract*—The opportunistic use of ambient radio-frequency (RF) signals for e-healthcare, smart living, security, and IoT applications has been attracting significant attention over the last years. Researchers and engineers have already proposed various approaches to integrate wireless communication with remote sensing by passively collecting Wi-Fi 2.4-GHz frequency band signals in indoor environments. Most of the existing passive sensing methods demand complex digital signal processing algorithms and/or adaptations to existent radio topology. In this paper, a passive microwave topology based on simultaneous injection-locking and injection-pulling of a RF oscillator for indoor passive sensing applications is presented. The direct-path signals from a source of RF waves and the signals that are phase-modulated by the target's motion are captured, combined, and fed into the injection-locking port of an oscillator. Due to the highly selective injection-locking for the stronger direct-path signal, and the injection-pulling behavior for the weaker scattered signal, the phase shifts of the electromagnetic waves that bounce off a moving target can be recovered. Experimental results demonstrate the feasibility of the proposed technique for microwave passive vital signs monitoring.**

Keywords— injection-locking, injection-pulling, oscillators, passive sensing, radar, vital signs monitoring, wireless sensing.

I. INTRODUCTION

Passive microwave sensing devices detect and track targets by simultaneously analyzing the direct-path signals emitted from RF sources and the signals scattered from targets of interest [1]-[4]. The use of passive RF sensors has a long history in military applications, airspace surveillance, and air traffic management. With the popularization of Wi-Fi-based wireless networks, different techniques that leverage access points (AP) as illuminators of opportunity for the passive recognition of targets have been proposed. The channel state information (CSI) and the received signal strength (RSS) are two major measurements used to take advantage of Wi-Fi signals for the passive detection of a target. However, RSS-based techniques face the major challenge of unforeseeable changes in the communication link due to the variety of ways in which the emitted RF signals bounce off objects and targets. On the other hand, CSI-based systems suffer from changes in the scene where the passive sensor is placed, so a training phase is always required whenever this protocol is utilized.

Conventional injection-locking-based technologies have already been used in passive sensing applications including vital sign detection and gesture identification [5]-[7]. The focus of existing injection-locked oscillator (ILO)-based approaches was to use the ILO to synchronize the frequency of its output signal with the frequency of a reference signal, which is usually the direct-path electromagnetic (EM) waves transmitted by an opportunistic source of microwave signals. Nonetheless, to the best of the authors' knowledge, the concurrent injection-locking and injection-pulling effects that arise when two microwave tones (unequal in power level) are fed on the injection-locking port of an ILO have not been exploited for the passive detection of a target of interest. In contrast to previous reported works, the proposed architecture may simplify the hardware requirements and increase the sensitivity of the system under potentially lower power consumption.

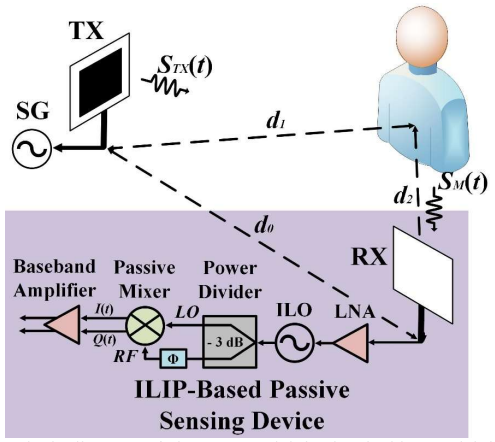

Fig. 1. Block diagram of the proposed injection-locking and injection-pulling based microwave passive sensing technique.

In this context, the authors have investigated the concurrent retrieval of both the transmitted signal from an ambient RF source and the signal scattered by a target for passive sensing applications in [8]-[9]. Therein, the internal asymmetric of the local-oscillator (LO)/RF ports of a nonlinear detector allowed the mixing of the two tones. In this paper, the proposed architecture is based on the injection-locking and injection-pulling of oscillators. The nonlinear detector allows the mixing of various tones that arise after the injection of the direct-path signals and the injection of the EM waves backscattered by a moving target into the ILO's input. Neither hardware modification nor previous synchronization to the RF source of direct-path signals is required. Only a light-weighted digital signal processing framework for the study of the baseband responses on the time and Fourier domains is needed to recover the desired Doppler information of a target of interest.

2023 International Microwave and Antenna Symposium (IMAS) | 978-1-6654-9075-7/23/$31.00 ©2023 IEEE | DOI: 10.1109/IMAS55807.2023.10066911

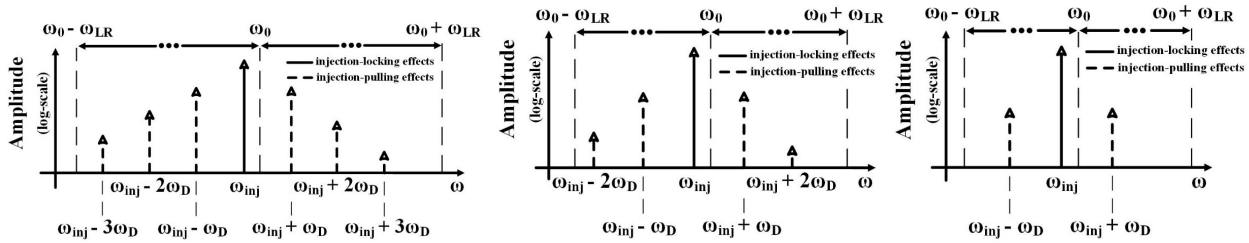

Fig. 2. Output spectrum of an oscillator under simultaneous injection-locking and injection-pulling effects (ω_{inj} = 2.4-GHz/ ω_D = 1 kHz). (a) -9 dB > α > - 13 dB. (b) -13 dB > α > - 23 dB. (c) -23 dB > α > - 50 dB, where $\alpha = P_{in}(\omega_{inj}+\omega_D)/P_{in}(\omega_{inj})$.

II. Injection-Locking and Injection-Pulling Mechanism Applied to Microwave Passive Sensing

Fig. 1 reveals the block diagram of the proposed passive sensing approach based on the concurrent injection-locking and the injection-pulling of a microwave oscillator. The technique leverages the ability of the ILO to synchronize to the direct-path signals (injection-locking) and a commonly undesirable behavior known as injection-pulling caused by the phase-modulated signals backscattered by a moving target. The Doppler frequencies associated with the target's movement can then be retrieved after mixing the products generated by the injection-locking and injection-pulling phenomena.

In contrast to conventional radar transceivers or other passive radar systems, the proposed device neither has an embedded microwave transmitter nor takes advantage of any dedicated antenna to recover the direct-propagation path signals of opportunity. As shown in Fig. 1, a signal generator (SG) operating at 2.4-GHz was used to mimic an ambient continuous-wave microwave signal source. Part of the transmitted signals of opportunity $S_{TX}(t)$ are phase-modulated by the target's movement and backscattered towards the injection-locking and injection-pulling (ILIP)-based passive sensing system ($S_M(t)$). In Fig. 1, the parameter d_0 represents the distance between the transmit (TX) and receive (RX) antennas, while the parameter d_1 is the distance between the TX antenna and the target. Finally, the separation between the system's RX antenna and the target is given by d_2.

After having its power level increased by the microwave amplifier(s) on the receiver chain, the received signal $S_{RX}(t)$ is fed into the injection port of the ILO. Assume that the frequency of the free-running oscillator before the injection-locking and the injection-pulling is ω_0, the locking range of the ILO is ω_{LR}, the frequency of the SG is ω_{inj}, and ω_D is the Doppler frequency associated with the detected periodic movement. To better illustrate the simultaneous injection-locking and injection-pulling mechanism, experiments were performed. Two tones with unequal power levels and centered at ω_{inj} = 2.4-GHz and $\omega_{inj}+\omega_D$ = 2.4-GHz + 1 kHz, respectively, were fed into the input of an ILO. The ratio between the power levels of both input signals is defined as the parameter α, i.e., $\alpha = P_{in}(\omega_{inj}+\omega_D)/P_{in}(\omega_{inj})$. Fig. 2(a) exhibits the spectrum at the ILO's output when -9 dB > α > - 13 dB, while Fig. 2(b) depicts the output spectrum when -13 dB > α > - 23 dB, and Fig. 2(c) illustrates the spectrum at the output of the ILO when -23 dB > α > - 50 dB. Let's define $P_{in}(\omega_{inj})$ as the power level of the direct-path signal and $P_{in}(\omega_{inj}+\omega_D)$ as the power level of the signals backscattered towards the

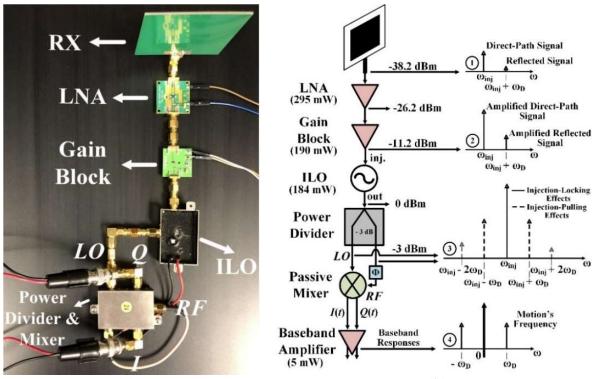

Fig. 3. (a) Photograph of the ILIP-based passive sensing device. (b) Estimated power level of the received direct-path signal at the input of each microwave module of the ILIP-based passive sensing device and the spectrum at four different key locations. The power consumption of each RF module is also exhibited.

passive sensing device. Based on the different values α may assume, the spectrum at the output of the ILO would be represented by one of the three profiles shown in Fig. 2(a), Fig. 2(b), and Fig. 2(c), respectively. In a realistic indoor environment, due to the significant power level difference between the reference signals (direct-path) and the backscattered signals, the profiles shown in Fig. 2(b) or Fig. 2(c) would likely represent the spectrum at the ILO's output. Therefore, considering that the three or five tones successively differing in frequency by ω_D (as depicted on Fig. 2(b) and Fig. 2(c), respectively) are simultaneous injected into the LO and RF ports of a microwave mixer, and leveraging the internal asymmetry of the RF and LO ports of the nonlinear detector, these tones will be mixed with themselves. Due to the conversion loss of the passive mixer, only the products of the mixing between the tones centered at $\omega_{inj} - \omega_D$ and at ω_{inj}, and the tones centered at $\omega_{inj} + \omega_D$ and at ω_{inj}, respectively, are obtained. The normalized-amplitude baseband outputs can be modeled as $I(t) = \cos(4\pi x(t)/\lambda + \delta)$ and $Q(t) = \sin(4\pi x(t)/\lambda + \delta)$, where $\lambda = f/c$ is the wavelength, f is the frequency of the radiated signals, c is the speed of light, and $\delta = 4\pi(-d_0 + d_1 + d_2)/\lambda$ is the phase delay associated with the direct-transmission path, the transmit antenna-target path, and the receive antenna-target path. $x(t) = msin(\omega_D t)$ is the periodic motion detected by the microwave passive system, where m is the motion's amplitude and ω_D is the motion's frequency. The recognition of the Doppler frequencies associated with a moving object is done by converting the baseband I/Q outputs into the Fourier domain.

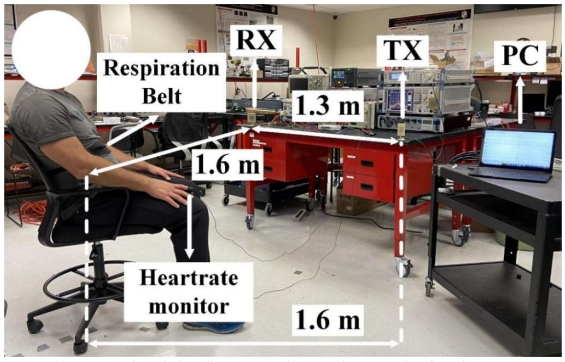

Fig. 4. Photograph of the first experimental scenario for the remote vital sign recognition using the proposed 2.4-GHz passive sensing system.

III. Experimental Results and Discussion

To evaluate the performance of the proposed microwave passive sensing approach, a 2.4-GHz ILIP-based passive sensing system (ILIP-PSD) was designed and experiments were conducted in two different setups. Fig. 3(a) illustrates the photograph of the proposed ILIP-based device. A 12-dB-gain low-noise amplifier (LNA) manufactured by RFMD (SGA4586Z) was employed on the front-end of the ILIP-based system. Its noise figure and its input referred P1dB at 2.4-GHz are 2.3 dB and -2.5 dBm, respectively. In addition, a gain block manufactured by Analog Devices (HMC311SC70) with gain, noise figure, and input referred P1dB of 15 dB, 5 dB and -1 dBm, at 2.4-GHz, respectively, was used to further boost the power level of the weak received signals. Since the LNA and the gain block are designed to operate from DC to 5 GHz and DC to 8 GHz, respectively, other coupled undesired signals might have potentially contributed an increment in the noise floor level. A power divider integrated with a microwave mixer functioned as a demodulator, and it was placed immediately after the last amplifier on the receiver chain. The power divider allows the uncoupling of the direct-path and phase-modulated received signals into the LO and RF inputs of a passive quadrature mixer optimized to operate at 2.4-GHz. A microwave cable was used to connect a signal generator (SG) to a 2.4-GHz antenna (TX). To mimic a realistic scenario, the transmitted power of the 2.4-GHz signal source was set to 19 dBm at the TX antenna port, which requires no additional hardware modification on the transmitter side of a general-purpose AP. The gain of the TX and RX antennas is 5.8 dBi. Finally, the power levels of the in-phase and quadrature *I*/*Q* signals, respectively, are further boosted by a baseband amplifier with a gain of 40 dB. The baseband responses were captured and converted to digital form using a data acquisition unit manufactured by DATAQ (DI-2108) with a sampling rate of 200-S/s.

Fig. 3(b) presents a schematic with the estimated power levels of the received direct-path signal at the input of each RF module of the ILIP-PSD, and the output spectrum at four key locations along the receiver chain. At location 1, the direct-path tone centered at ω_{inj} and the phase-modulated tone centered at $\omega_{inj}+\omega_D$ are exhibited. Both signals are shown in location 2 after having their power level boosted by the receiver's amplification chain. At location 3, the spectrum at the outputs of the power divider is depicted. It should be noted that these tones centered at $\omega_{inj}-\omega_D$, ω_{inj}, and $\omega_{inj}+\omega_D$, respectively, are the products of the simultaneous injection-locking and injection-pulling effects. Tones centered at $\omega_{inj}-2\omega_D$ and $\omega_{inj}+2\omega_D$ may also appear. Finally, the spectrum of the baseband responses is illustrated at location 4. The DC power consumption of each RF module is also shown in Fig. 3(b).

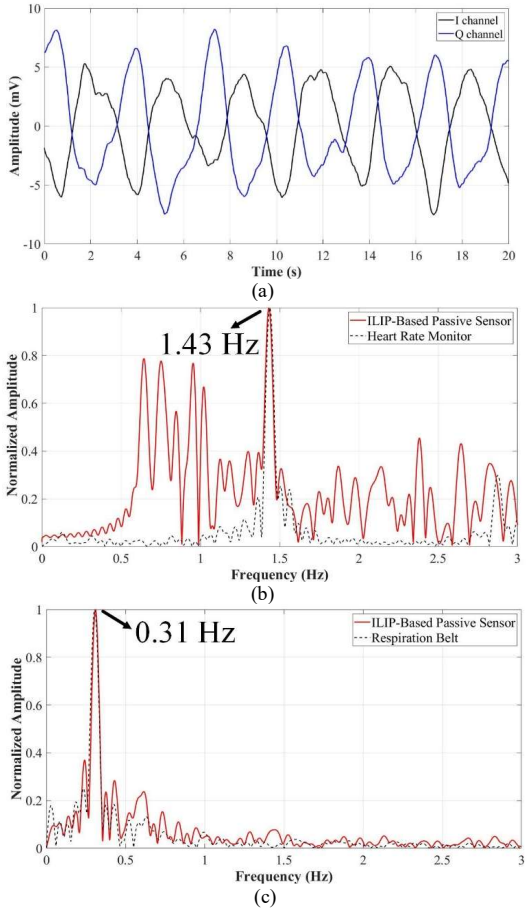

Fig. 5. Spectrum of the low-pass filtered *I*/*Q* baseband signals and the respiration belt's output when the human subject is seated 1.6 m away from the illuminator of opportunity and the ILIP-based passive sensing system, respectively.

Fig. 4 details the first experimental setup used to demonstrate the vital sign detection of a stationary human target. The RF signals transmitted by an illuminator of opportunity are phase-modulated by the chest movements caused by the subject's cardiopulmonary activities. Part of the backscattered phase-modulated signals are retrieved by the RX antenna. By comparing the direct-path and the backscattered EM waves, the frequencies associated with the thoracic surface motion can be retrieved. The distance between the TX and RX antennas were 1.3 m, and the distances between the human target and the RX and TX antennas were 1.6 m, respectively. A fingertip pulse monitor was used to provide the groundtruth for the heart rate, while a respiration belt was used to provide the groundtruth for the breathing rate. Fig. 5(a) presents the time-domain responses retrieved by the ILIP-PSD when the person is seated still in front of the sensing mechanism. The time-domain signatures were smoothed by a moving-average approach with 100-element sliding window. To highly attenuate the powerful harmonic component associated with the breathing motion, a high-pass filter with cut-off frequency of 0.65 Hz is applied to

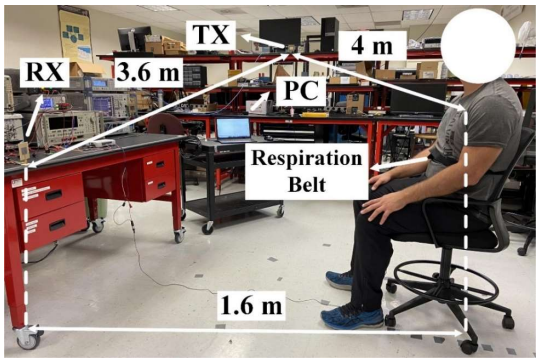

Fig. 6. Photograph of the second experimental scenario for the remote vital sign recognition using the proposed 2.4-GHz passive sensing system.

the raw *I*/*Q* baseband signals. By doing this, the much weaker tone associated with the heartbeat can be identified. Fig. 5(b) shows the spectrum of the high-pass filtered *I*/*Q* baseband signals and the spectrum of the simultaneously retrieved heart rate monitor's output. The heart rate is estimated by both sensors as 1.43 Hz, which is equivalent to 85.80 bpm. To estimate the frequency of the harmonic component associated with the respiration motion, a 0.65-Hz lowpass filter was applied to the baseband signals. Fig. 5(c) depicts the spectrum of the low-pass filtered baseband response and the spectrum of the simultaneously retrieved respiration belt's output. The respiration rate was estimated by both sensors as 0.31 Hz, which converts to 18.6 breaths/min. Both the heartbeat and respiration rate measurements are in agreement with the corresponding groundtruth measurements.

To further evaluate the sensitivity of the proposed microwave passive sensor for vital sign monitoring, the experimental scene was changed as shown in Fig. 6. The distances between the TX and the RX antennas were increased to 3.6 m, and the distance between the TX antenna and the human subject was increased to 4 m. The distance between the RX antenna and the human subject was kept as 1.6 m. The transmitted power of the 2.4-GHz signal source was measured as 16 dBm at the TX antenna input port. Fig. 7(a) plots the time-domain baseband responses that mainly corresponds to the respiration motion performed by a person seated still in front of the ILIP-PSD. In Fig. 7(b), the spectrum of the low-pass filtered *I*/*Q* baseband signals and the respiration belt's output when the human subject is seated 4 m away from the illuminator of opportunity and 1.6 m away from the ILIP-based passive sensing system is exhibited. The respiration measurement retrieved by the ILIP-PSD and the respiration belt were estimated as 0.29 Hz (17.4 breaths/min), and the second harmonic of the tone associated to the respiration motion can also be seen in Fig. 7(b).

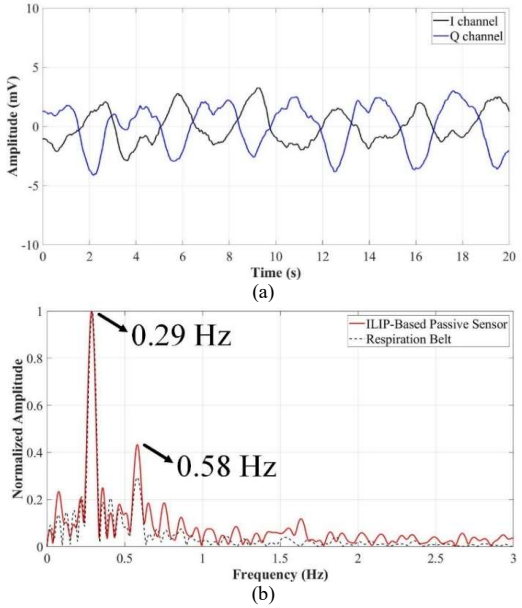

Fig. 7. (a) *I*/*Q* baseband signals and (b) spectrum of the low-pass filtered *I*/*Q* baseband signals and the respiration belt's output when the human subject is seated 4 m away from the illuminator of opportunity and 1.6 m away from the ILIP-based passive sensing system.

IV. Conclusion

In this paper, a novel ILIP-based microwave architecture that leverages ambient RF radiations from a source of electromagnetic signals for passive sensing is presented. By concurrently feeding the direct-path ambient signals and the phase-modulated signals backscattered from the target of interest into the input of an injection-locked oscillator, the injection-locking and the injection-pulling mechanisms successfully allows the detection of the vital signs of a person seated in front the ILIIP-PSD. After being optimized and fully integrated, the proposed sensor has the potential for several industrial and consumer applications, including passive vital sign tracking, passive presence detection, and passive gesture control.

Acknowledgment

The authors wish to acknowledge National Science Foundation (NSF) under ECCS-2030094 and ECCS-1808613.

References

[1] Z. Pu, M. Zhu, W. Li, Z. Cui, X. Guo and Y. Wang, "Monitoring public transit ridership flow by passively sensing Wi-Fi and Bluetooth mobile devices," *IEEE Internet of Things J.*, vol. 8, no. 1, pp. 474-486, 1 Jan.1, 2021.

[2] Y. Liu, T. Wang, Y. Jiang and B. Chen, "Harvesting Ambient RF for Presence Detection Through Deep Learning," *IEEE Trans. Neural Netw. Learn. Syst.* (early access).

[3] W. Li, M. J. Bocus, C. Tang, R. J. Piechocki, K. Woodbridge and K. Chetty, "On CSI and passive Wi-Fi radar for opportunistic physical activity recognition," *IEEE Trans. Wirel. Commun.*, vol. 21, no. 1, pp. 607-620, Jan. 2022.

[4] W. Li, B. Tan, and R. Piechocki, "Passive radar for opportunistic monitoring in e-health applications," *IEEE J. Transl. Eng. Health Med.*, vol. 6, pp. 1–10, 2018.

[5] M. Tang, F. Wang and T. Horng, "Vital-sign detection based on a passive WiFi radar," in *Proc. IEEE MTT-S International Microwave Workshop Series on RF and Wireless Technologies for Biomedical and Healthcare Applications (IMWS-BIO)*, pp. 74-75, 2015.

[6] F. Wang, M. Tang, Y. Chiu and T. Horng, "Gesture sensing using retransmitted wireless communication signals based on Doppler radar technology," *IEEE Trans. Microw. Theory Tech.*, vol. 63, no. 12, pp. 4592-4602, Dec. 2015.

[7] Y. Lai, C. Chou, M. Tang, T. Horng and F. Wang, "Finger gesture sensing and recognition using a Wi-Fi-based passive radar," in *Proc. IEEE MTT-S International Microwave Symposium (IMS)*, pp. 293-296, 2019.

[8] D. V. Q. Rodrigues, D. Tang and C. Li, "A Novel Microwave Architecture for Passive Sensing Applications," in *Proc. IEEE Radio and Wireless Symposium (RWS)*, 2022, pp. 57-59.

[9] D. Tang, V. G. R. Varela, D. V. Q. Rodrigues, D. Rodriguez and C. Li, "A Wi-Fi Frequency Band Passive Biomedical Doppler Radar Sensor," *IEEE Trans. Microw. Theory Techn.,* 2022.